Magnetically Geared Pseudo Direct Drive for Safety Critical Applications

R. S. Dragan[1], R. E. Clark[1], E. K. Hussain[2], K. Atallah[2], M. Odavic[2]
[1]Magnomatics Ltd., Sheffield, United Kingdom, r.dragan@magnomatics.com
[2]Department of Electronic and Electrical Engineering, University of Sheffield, Sheffield, United Kingdom

Abstract—The paper presents an investigation into the electromagnetic design and performance of a fault-tolerant magnetically geared Pseudo Direct Drive (PDD®) electrical machine for primary flight control surface electromechanical actuation. It is shown that a large number of combinations of high-speed rotor (HSR) pole pairs, pole-piece numbers, and stator slot numbers exist for which a duplex 3-phase fault tolerant configuration can be realized. Furthermore, in addition to facilitating a lower mass solution, it is also shown that a PDD presents a significantly lower inertia referred to the screw, when compared to direct-drive or mechanically geared motor solutions. The findings are validated on a prototype PDD, which has been designed and built to meet the requirements of a primary control surface electromechanical actuator.

Keywords—magnetic gear, brushless machine, aerospace

I. INTRODUCTION

The paper presents an investigation into the electromagnetic design and performance of a fault-tolerant magnetically geared Pseudo Direct Drive (PDD®) electrical machine for primary flight control surface actuation. "Power-by-wire" actuators used in aircraft flight control surface actuation can be divided into electro-hydrostatic, EHA, and electromechanical, EMA. The typical architecture of an EHA consists of an electric motor driven pump which supplies a hydraulic cylinder. EHAs are currently preferred due to their high power density, good damping characteristics and reduced jamming probability [1]. In contrast, the EMA drive train topology consists of a high speed electrical motor connected to the ball/roller screw through a mechanical reduction gearbox. Although such designs exhibit high power density, efficiency, and improved dynamic performance, their susceptibility to jamming events is still higher than other actuator technologies, which can be caused by failures in the mechanical drive train including the gearbox, screw etc. These failures could be caused by a combination of shock loads, such as wind gusts and object strikes, and the kinetic energy of the rotor of the electrical machine. Furthermore, although the high gear ratio of the mechanical gearbox in EMAs has the benefit of reducing the size/mass of the electrical machine, it often results in increased kinetic energy in the rotor of the electrical machine. The fault tolerant PDD, Fig. 1, consists of a magnetically and mechanically integrated brushless permanent magnet motor and a magnetic gear (MG) [2]. The inner high speed rotor (HSR) of the PDD interacts with the stator windings to produce torque, which is transmitted to the output pole piece rotor (PPR) through the interaction between the stationary permanent magnets on the stator, and the asynchronous space harmonic resulting from the modulation of the fields of the permanent magnets on the HSR by the pole-pieces on the output rotor [3,4]. By employing a PDD, the mechanical gear stages of the actuator drive train can be reduced or completely, removed and the HSR of the PDD is now directly connected to the mechanical drive train through the magnetic gear element. Due to its inherent compliance and torque limiting characteristics, the magnetic gear element effectively isolates the mechanical drive train from the effects of the kinetic energy stored in the high-speed rotor. It is shown that for actuator applications, while the PDD exhibits half the mass, the inertia of the rotor in contact with the mechanical drivetrain can be an order of magnitude smaller than that of an equivalent conventional permanent magnet (PM) machine. It is also shown that despite the compliance of the magnetic gear element of the PDD, the required actuator bandwidths are easily achieved and exceeded.

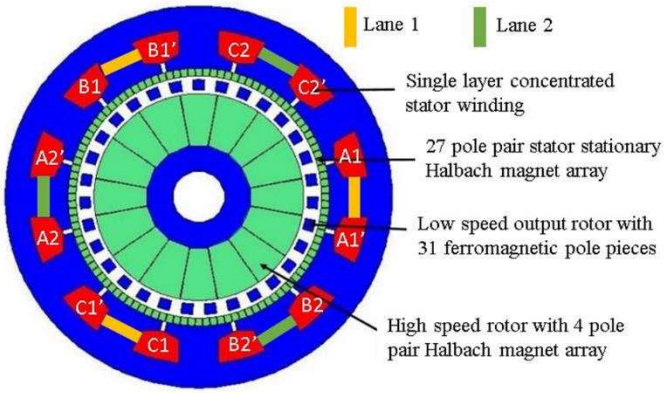

Fig. 1. Fault tolerant PDD topology

II. STORED ENERGY IN DIRECT DRIVE, MECHANICALLY GEARED AND MAGNETICALLY GEARED MACHINES

A large percentage of linear EMA topologies are based on a PM machine which is connected to the screw of the actuator via a reduction gearbox, in order to reduce the motor torque requirement and hence overall mass. However, in contrast to a direct drive system, the geared drivetrain topology is more

978-1-5090-4281-4/17/$31.00 ©2017 IEEE

complex, and often results in a larger stored kinetic energy in the rotor of the machine [5]. By considering the inertia associated with the output rotors of a conventional PM and PDD motor, it can be shown that the kinetic energy stored in a PM motor mechanically geared actuation system is several times higher than the one in a PDD based actuation drivetrain. For ease of comparison, both actuation drivetrain topologies, conventional PM and PDD electrical machines, are considered to have a mechanical gear within their drivetrain and are compared with a PM direct drive topology. The output rotor inertia of an electrical machine can be expressed as a function of density and diameter of the rotor, ρ_{mg} and D_{mg} with β being the aspect ratio of active length, L, over diameter.

$$I_{mg} = \frac{\pi \rho_{mg} \beta D_{mg}^5}{32} \quad (1)$$

The energy stored in the output rotor of a mechanically geared electrical machine, with an angular velocity $\omega_{mg} = G_{rm}\omega_L$, when referred to actuator control surface side, through the mechanical gear ratio, G_{rm}, is given by (2):

$$E_{mg} = \frac{1}{2}\frac{\pi \rho_{mg} \beta}{32} D_{mg}^5 \omega_L^2 G_{rm}^2 \quad (2)$$

In contrast, the energy stored in the output rotor of a direct drive machine, of similar rotor topology, can be expressed as:

$$E_{DD} = \frac{1}{2}\frac{\pi \rho_{DD} \beta}{32} D_{DD}^5 \omega_L^2 \quad (3)$$

where D_{DD} and ρ_{DD} represent the diameter and density of the rotor of the direct drive electrical machine. The ratio between the diameter of the rotor of the mechanically geared and direct drive machine can be expressed as a function of the airgap shear stress such that:

$$\frac{D_{mg}}{D_{DD}} = \sqrt[3]{\frac{\sigma_{DD}}{\sigma_{mg} G_{rm}}} \quad (4)$$

where σ_{mg} and σ_{DD} represent the airgap shear stress of the geared and direct drive electrical machines, and assuming these to be equal, the energy ratio between the mechanically geared and direct drive systems (PMDD), considering that the same torque is produced at the input of the screw, and for the same aspect ratio, β, is given by:

$$\frac{E_{mg}}{E_{DD}} = G_{rm}^{1/3} \quad (5)$$

Similarly, the ratio of energy of the PPR of a PDD to the energy of a direct drive, for the same output torque and aspect ratio, β, can be expressed as:

$$\frac{E_{PDD}}{E_{DD}} = \frac{\rho_{PDD}}{\rho_{DD}} \left(\frac{\sigma_{DD}}{\sigma_{PDD}} \right)^{5/3} G_{rm}^{1/3} \quad (6)$$

where, ρ_{DD}, σ_{DD} and ρ_{PDD}, σ_{PDD} are the densities of the output rotors and airgap shear stresses of the direct drive PM and PDD electrical machines, respectively.

The airgap shear stress of the conventional surface mount PM machine considered in this comparison was calculated at $\sigma_{DD} = 13\text{kPa}$, while for the PDD a value of $\sigma_{PDD} = 52\text{kPa}$ was evaluated for the same output torque. Fig. 2 shows the variation of the energy of the conventional PM and PDD systems as per unit of that of PM direct-drive. It can be seen that for the same mechanical gear ratio between the machine and screw, the energy stored due to the inertia of the low speed rotor of a PDD is significantly less than the energy stored in a conventional PM machine. This is mainly due to the structure of the PPR and the larger airgap shear stress of the PDD.

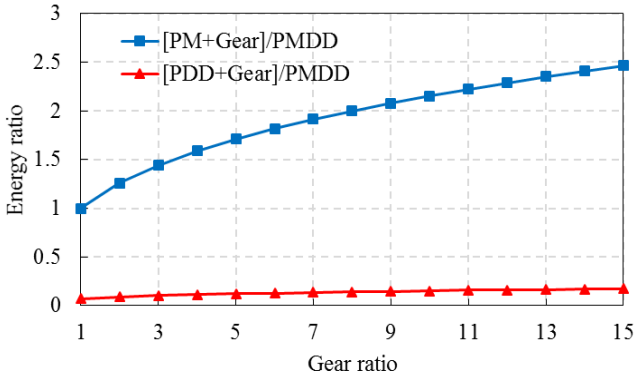

Fig. 2. Variation of energy stored in the output rotor

III. SELECTION OF PDD DESIGN PARAMETERS

A. Winding configuration

In order to achieve fault tolerance, each sub-system (i.e. electrical machine, power electronics) has to have built-in redundancy such that the maximum failure/hazard rate is not exceeded. Typically, a fault tolerant electrical machine has multiple physically, magnetically, electrically and thermally isolated phases or sets of phases, each capable of producing rated torque in the event of failure. In [9] the relative hazard rates of different fault tolerant configurations were compared and it was shown that the duplex 3-phase winding configuration, supplied from duplex 3-phase conventional 6-switch field oriented control converters, exhibits the lowest hazard rate, Fig. 3.

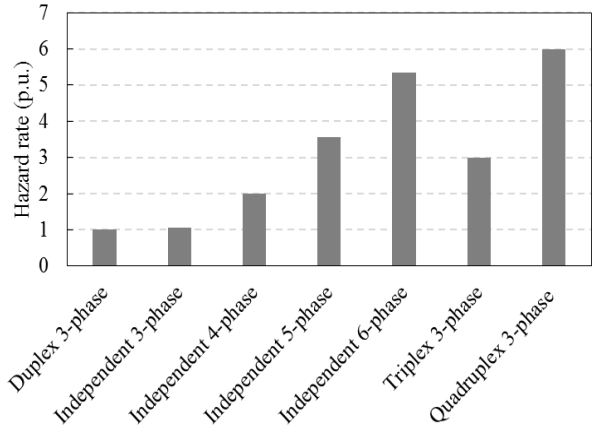

Fig. 3. Hazard rate of fault tolerant configurations

B. Slot-pole combinations and gear ratios

A PDD consists of a brushless PM machine mechanically and magnetically integrated with a magnetic gear, and in this configuration, the HSR and PPR represent the input and output rotors of the PDD magnetic gear element. The outer stator houses the windings, and provides mechanical support for the outer magnet array which is fixed to its bore. The gear ratio between the HSR and the PPR, G_r is given in [10] by:

$$G_r = \frac{N_{pp}}{p_h} = 1 + \frac{p_l}{p_h} \quad (7)$$

where p_l, p_h and N_{pp} are the pole-pairs of the magnet arrays mounted on the stator and HSR and the number of pole pieces on the PPR, respectively. The electromagnetic torque of the PDD, T_e, or input torque of the magnetic gear is produced by the synchronous coupling of the HSR fundamental field component with the fundamental of the stator MMF and can be expressed as:

$$T_e = \frac{3}{2} p_h \varphi_m i_q \quad (8)$$

where φ_m and i_q are the fundamental flux linkage and q-axis current, respectively. The transmitted torque, T_o is given by:

$$T_o = G_r \left(T_e - J_h \frac{d^2\theta_h}{dt^2} \right) = G_r \left(\frac{3}{2} p_h \varphi_m i_q - J_h \frac{d^2\theta_h}{dt^2} \right) \quad (9)$$

J_h and θ_h are the inertia and the angular position of the HSR, respectively.

The duplex 3-phase concentrated single layer winding configuration can be realized by selecting the appropriate combinations of the numbers of pole-pairs of the PM arrays on the HSR and the stator, the pole-pieces on the PPR, and the number of stator slots. Firstly, the numbers of pole-pairs on the HSR and the number of stator slots are selected in order to achieve the duplex 3-phase fault tolerant brushless machine element, then the numbers of pole-pieces and pole-pairs of the stationary PMs are selected in order to achieve the required gear ratio. For 12 stator slots, which can accommodate a duplex 3-phase winding, Table I gives the possible combinations of pole-pairs on the HSR and stator and the number pole-pieces. It can be seen that for 12 stator slots a large number of combinations exist.

For the 2D cross-section presented in Fig. 1, Fig. 4 shows the variation of the pull-out torque on the PPR rotor, with the gear ratios from Table I, for a fixed magnet mass on the HSR and stator. It can be seen that as the gear ratio is increased, the pull-out torque is reduced. Fig. 5 shows the cogging torque on the output rotor for the different gear ratios. The integer gear ratios which have a cogging torque factor larger than 1, exhibit a relatively larger cogging torque [11].

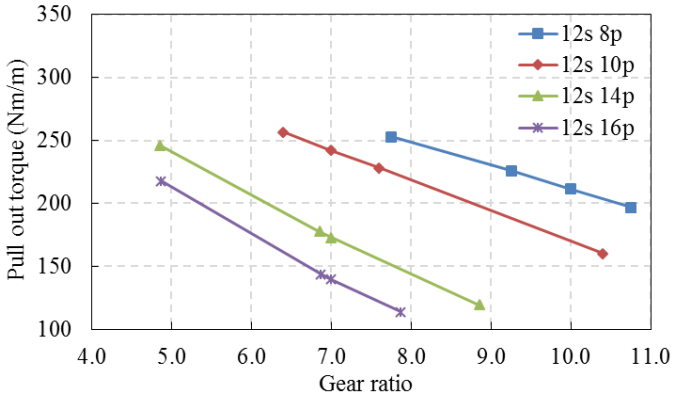

Fig. 4. Variation of pull-out torque with gear ratio for a fixed magnet mass

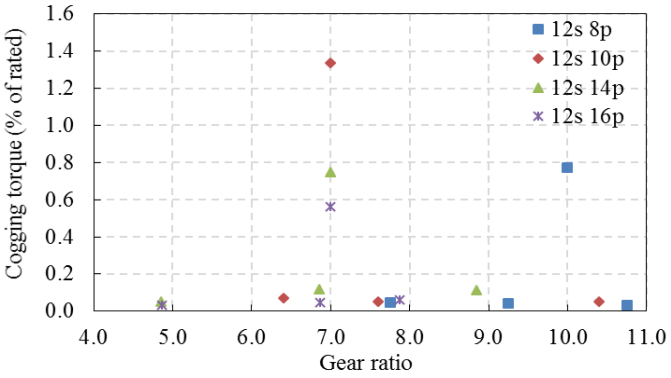

Fig. 5. Variation of cogging torque with gear ratio

Table I. Fault tolerant PDD machine topologies

Stator slots	12															
Number of pole-pairs on HSR	4				5				7				8			
Gear Ratio	7.75	9.25	10	10.75	6.4	7.0	7.6	10.4	4.86	6.86	7.0	8.86	4.88	6.88	7.0	7.9
PM pole-pairs stator	27	33	36	39	27	30	33	47	27	41	42	55	31	47	48	55
Cogging torque factor [5]	1	1	4	1	1	5	1	1	1	1	7	1	1	1	8	1

In order to investigate the effects of the leading design parameters, for the gear ratios highlighted in Table I, the volume of the permanent magnets on the HSR and stator are varied together with the ratio of the radial to circumferential components for the discrete Halbach magnetization on the HSR. Furthermore, in the analysis the radial and circumferential thicknesses of the pole-pieces and the slot depth, are also varied. For a given PPR diameter, the designs with the lowest PPR inertia are selected, and the variation of the PPR inertia and the corresponding active mass of the PDD are shown in Fig. 6 and Fig. 7, respectively. It can be seen, that an optimum PPR diameter exists for which its inertia is minimum. It can also be observed that the 12 slots 8 pole design exhibits the lowest active mass. Therefore, a design that meets the mass requirement with the lowest inertia was selected.

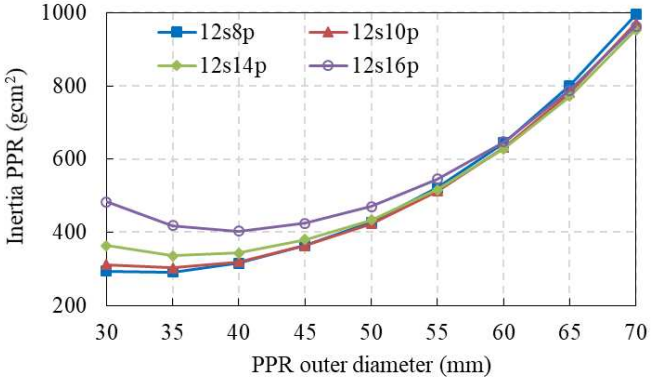

Fig. 6. Variation of the output rotor inertia with PPR diameter

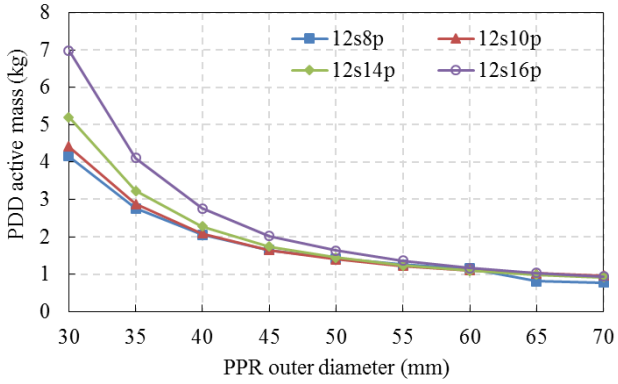

Fig. 7. Variation of the PDD active mass with PPR diameter

C. Magnetic gear torque response time

The PDD torque response time is represented by the electrical time constant of the electrical machine as well as the magnetic gear (MG) element torque transmission response time. The electrical time constant, t_e, is the time required for the current in the windings to rise to the demanded value in order to produce the required torque on the HSR of the PDD and is given by:

$$t_e = \frac{L_{ph}}{R_{ph}} \tag{10}$$

where L_{ph} and R_{ph} are the phase inductance and resistance.

The MG element torque response time is the duration taken to transmit, the electromagnetic torque from the HSR to the output PPR, through the compliant transmission. The torque transmission capability of a 12s8p design is shown in Fig. 8. It can be observed that the transmitted torque is determined by the relative positions of the HSR and PPR. Thus, the HSR must move in order to transmit the geared electromagnetic torque to the PPR and the relative load angle between the two rotors, θ_e, is given by:

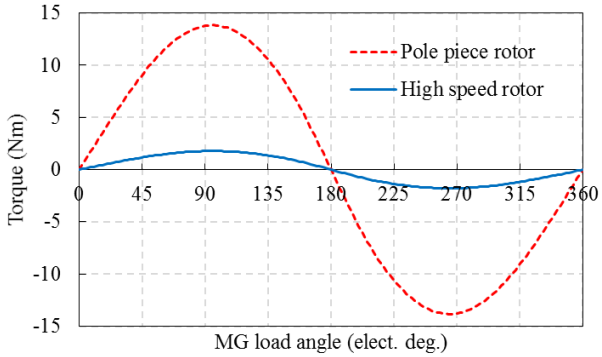

Fig. 8 Variation of transmitted geared torque with MG load angle. (rated value at 57 elec. deg.)

$$\theta_e = p_h\theta_h - N_{pp}\theta_{pp} \tag{11}$$

Furthermore, when the rated torque,T_r, of the HSR is applied, the equation governing the motion of the HSR is given by:

$$J_h\frac{d\omega_h}{dt} = T_r - \frac{T_m}{G_r}\sin(p_h\theta_h - N_{pp}\theta_{pp}) \tag{12}$$

For simplicity, by assuming the PPR remains static, i.e. $\theta_{pp} = 0$, equation (12) becomes:

$$\frac{d^2\theta_h}{dt^2} = \frac{T_r}{J_h} - \frac{T_m}{J_h G_r}\sin(p_h\theta_h) \tag{13}$$

where T_m is the PPR pull-out torque.

And assuming, for simplicity, that when, $0 \le \theta_h \le \frac{1}{p_h}\sin^{-1}\left(G_r\frac{T_r}{T_m}\right)$, the transmitted torque varies linearly with the load angle, and at the rated conditions :

$$T_r = \frac{k}{p_h}\sin^{-1}\left(G_r\frac{T_r}{T_m}\right) \tag{14}$$

where k is a constant given by:

$$k = \frac{T_r\, p_h}{\sin^{-1}\left(\frac{T_r G_r}{T_m}\right)} \tag{15}$$

By substituting (14) in (13):

$$\frac{d^2\theta_h}{dt^2} + \frac{k}{J_h}\theta_h = \frac{T_r}{J_h} \tag{16}$$

By applying the boundary conditions where at $t = 0$, $\theta_h = 0$ and $\frac{d\theta_h}{dt} = 0$, the variation of θ_h with time is then given by:

$$\theta_h(t) = \frac{T_r}{k}\left(1 - \cos\left(\sqrt{\frac{k}{J_h}}t\right)\right) \tag{17}$$

The time taken to transmit the electromagnetic torque from the HSR to the PPR can be approximated by substituting (14) and (15) in (17) such that:

$$t = \frac{\pi}{2}\sqrt{\frac{J_h \sin^{-1}\left(\frac{T_r G_r}{T_m}\right)}{T_r p_h}} \quad (18)$$

For the designs in Fig. 6, the time taken for the MG element to transmit the rated torque to the output rotor is shown in Fig. 9. It can be observed that for all designs, the delay is less than 12ms, being smaller for smaller gear ratios.

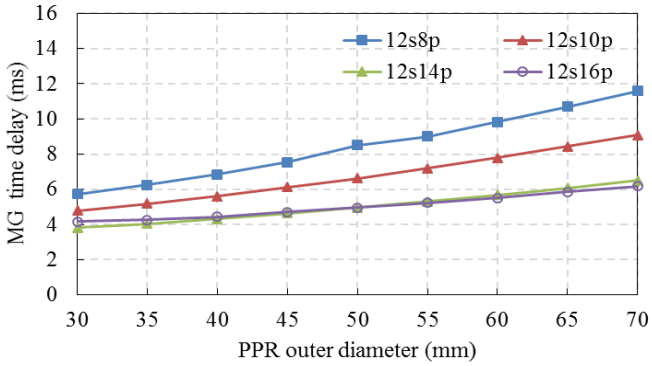

Fig. 9. Variation of MG time delay with PPR outer diameter for different gear ratios

D. Actuator Bandwidth

The actuator drivetrain comprises the fault tolerant PDD which drives the linear power screw, which is connected to the primary control surface. The bandwidth of the actuator, can be analytically predicted by considering the PDD output torque and load torque on the surface, and the equivalent inertias of the PDD rotors, linear screw and control surface. For a sinusoidal angular position, θ, of the PPR:

$$\theta(t) = \theta_m \sin(\omega t) \quad (19)$$

where ω and θ_m represent the PPR frequency and maximum angular position at the particular frequency.

Due to the very short time it takes for torque to be transmitted to the PPR, Fig. 9, compared to the required bandwidth, Fig. 10, torque transmission transients are neglected and the PDD output torque is approximated by $T_e\ G_r$. Thus,

$$-J_T \theta_m \omega^2 \sin(\omega t) = G_r\ T_e(t) - T_L \quad (20)$$

where T_L is the load torque given by the aerodynamic loading of the control surface and J_T is the total system inertia. Since the aerodynamic load torque for this specific actuator is proportional to the angular position, a ratio between the absolute maximum load torque, T_{L_MAX}, and angular position, θ_m, can be defined by:

$$C = \frac{T_{L\_MAX}}{\theta_m} \quad (21)$$

where θ_m is related to the maximum linear displacement of the slide, X_m, of the linear screw such that:

$$\theta_m = \frac{2\pi X_m}{\lambda} \quad (22)$$

where λ is the lead of the power screw. Equation (20) becomes:

$$-J_T \theta_m \omega^2 \sin(\omega t) = G_r\ T_e(t) - C\theta_m \sin(\omega t) \quad (23)$$

Therefore, at maximum displacement, θ_m:

$$(C - J_T \omega^2)\theta_m = G_r T_x \quad (24)$$

From equations (22) and (24), the variation of the bandwidth of the actuator with the maximum displacement, X_m, is given by:

$$f = \frac{1}{2\pi}\sqrt{\frac{\left(C - \frac{G_r T_x \lambda}{2\pi X_m}\right)}{J_T}} \quad (25)$$

Where $T_x = T_r$, when $\left(C - G_r \frac{T_r}{\theta_m}\right) \geq 0$, and $T_x = -T_r$ when $\left(C - G_r \frac{T_r}{\theta_m}\right) < 0$.

In order to calculate the total system inertia, J_T, the HSR inertia has to be referred through the magnetic gear to the output side and added to the load, screw and PPR inertias, J_L, J_{screw} and J_{PPR}, respectively, such that:

$$J_T = J_L + J_{screw} + J_{PPR} + J_{HSR} G_r^2 \quad (26)$$

However, the speed of the HSR is limited to $\omega_{HSR-MAX}$ and f must also satisfy:

$$\omega_{HSR-MAX} \geq \frac{4\pi^2 X_m f}{\lambda} G_r \quad (27)$$

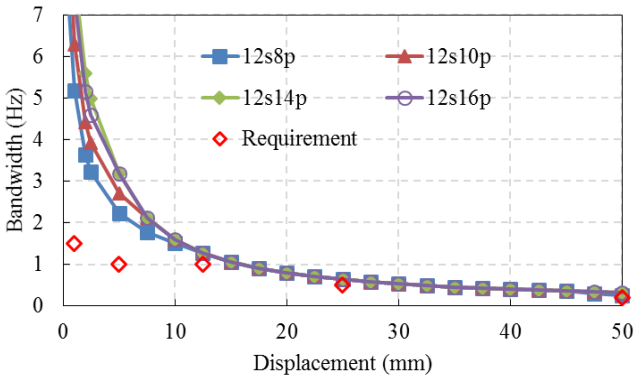

Fig. 10. Variation of PDD bandwidth with displacement for 45mm PPR outer diameter designs

The analytically predicted bandwidths of the selected PDD slot pole combinations and corresponding gear ratios highlighted in Table I, for a PPR outer diameter of 45mm, are compared in Fig. 10 with the bandwidth requirement of a rudder control surface actuator system. It can be observed that all the PDD designs are able to surpass the requirement for displacements smaller than 10mm.

IV. ANALYSIS AND DESIGN REFINMENT OF SELECTED PDD

A. Inductance

The 12 slot 8 HSR poles, 7.75:1 PDD topology, Fig. 1, was selected for prototyping with a 3-phase duplex winding configuration, with each lane capable of producing rated power. The phase inductance was designed to be 1 p.u. in order to limit the terminal short circuit current to the rated current. Since the

magnetic gear element of the PDD is optimised for minimum inertia and mass, the phase inductance was adjusted to a 1 p.u. value by adjusting the slot opening length, A, and the tooth tip height, B, Fig. 11.

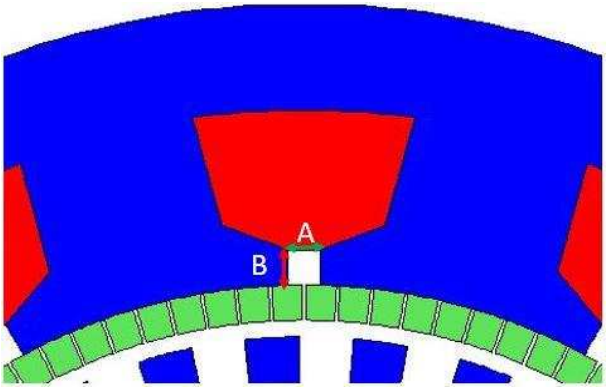

Fig. 11. Slot opening dimensions

The variation of phase inductance with the tooth tip thickness for several slot opening lengths is presented in Fig. 12. In order to support the stator mounted PMs, the slot opening was constrained to a minimum value of 0.9mm. A design with 1p.u. inductance was selected, such that during a 3-phase short circuit of one lane, the short circuit current is limited to the rated value of the phase current, limiting the copper loss of the faulted lane and allowing the electrical machine to continue operation using the redundant healthy lane.

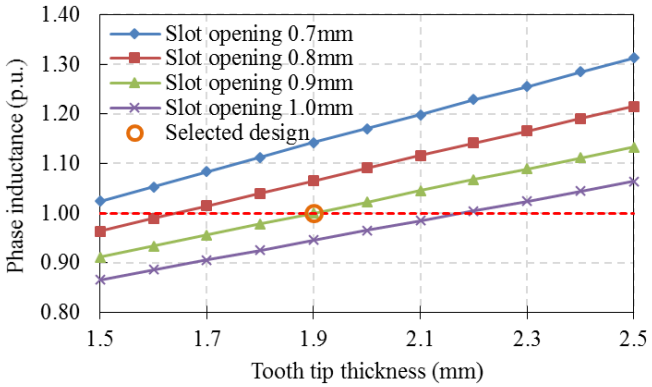

Fig. 12. Variation of phase inductance

B. Losses

The losses in the PDD prototype can be divided into copper losses, which are essentially torque dependent, and iron and eddy current losses, which are essentially speed dependent. The latter, include the iron losses in the SiFe stator laminations, and the eddy current losses in the stator PMs, the stator Titanium sleeve, which secures the stator PMs, and the solid SiFe pole-pieces. All the losses have been predicted with the permanent magnets and copper at a temperature of 80ºC.

The iron losses in the stator have been calculated from a set of 2D FE magnetostatic solutions. The hysteresis component of the stator iron loss is given by:

$$W_{hys} = k_h \frac{1}{T} B_m^{a+bB_m} \quad \left(\frac{W}{kg}\right) \tag{28}$$

where k_h, a and b are material constants and B_m represents the peak magnetic flux density. The classical eddy current loss component for the laminated stator stack, for the electrical period, T , can be calculated from:

$$P_{cl} = \frac{d^2}{\rho \cdot f \cdot 12 \cdot \delta} \cdot \frac{1}{T} \int_0^T \left(\frac{dB}{dT}\right)^2 dt \quad \left(\frac{W}{kg}\right) \tag{29}$$

where d is the lamination thickness, ρ is the electrical resistivity, δ is the density of the lamination material, f is the electrical frequency of the HSR. The excess eddy current loss is given by:

$$P_{ex} = \frac{k_{ex}}{T} \int_0^T \left|\frac{dB}{dt}\right|^{1.5} dt \quad \left(\frac{W}{kg}\right) \tag{30}$$

where k_{ex} is a material constant .

The eddy current losses in the non-laminated permanent magnet arrays, pole pieces and outer magnet Titanium retention sleeve were obtained from a 3D FE transient model.

The stator iron loss for the fault tolerant PDD with a duplex 3-phase winding operating in either an Active-Passive or Active-Active mode is presented in Fig. 13. Fig. 14 shows the total eddy current loss is the solid PDD components. In the analysis, it is assumed that the effect of load on the eddy current loss is negligible, and is mainly affected by the HSR/PPR speed.

The copper loss was obtained by considering the RMS phase current, I_{rms}, and phase resistance R_{phase} of one lane of the duplex 3-phase configuration. The copper loss for each lane is given by:

$$P_{copper} = 3 I_{rms}^2 R_{phase} \quad (W) \tag{31}$$

The copper loss of the fault tolerant PDD prototype was adjusted in order to take into consideration the reduction of the EMF due to 3D effects and the machine operating temperature.

Fig. 15 shows the variation of the copper losses with torque, for the Active-Passive and Active-Active modes of operation. Fig. 16 and 17 show the efficiency maps for Active-Passive and Active-Active modes of operation. It can be seen that an Active-Active operation is more efficient. Fig. 18 shows the efficiency map for the Active-Active mode when the eddy current loss in the Titanium sleeve is removed and the solid pole pieces are manufactured from laminated SiFe steel. It can be seen that the efficiency is significantly improved. However, the speed dependent eddy current losses can significantly improve the controllability, as passive dampers, especially during air turbulence/gusts and following object strike events. This can also result in a smaller dump resistor connected to the dc link of the 3-phase converter of the electrical machine.

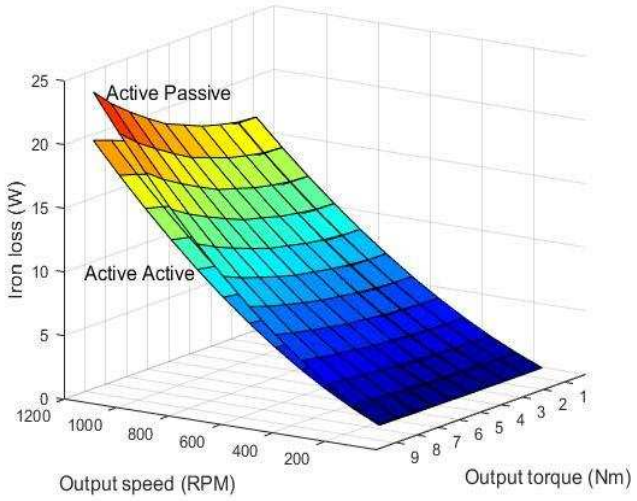

Fig. 13. Stator iron loss Active-Passive / Active-Active

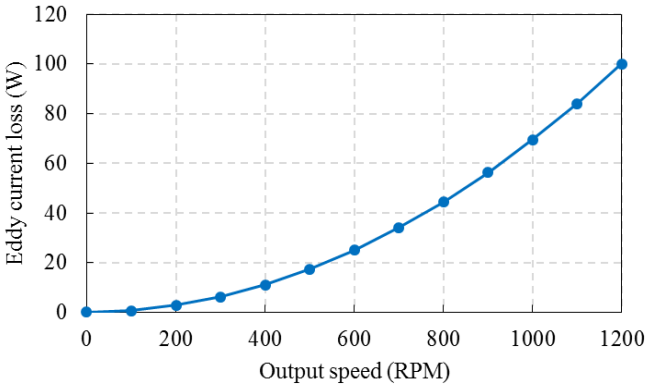

Fig. 14. Eddy current loss in solid components

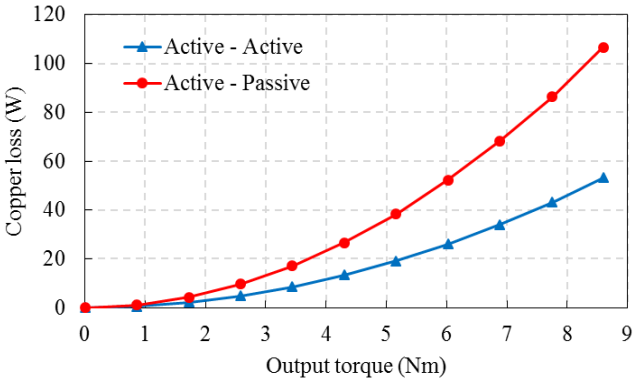

Fig. 15. Copper loss Active-Passive / Active-Active

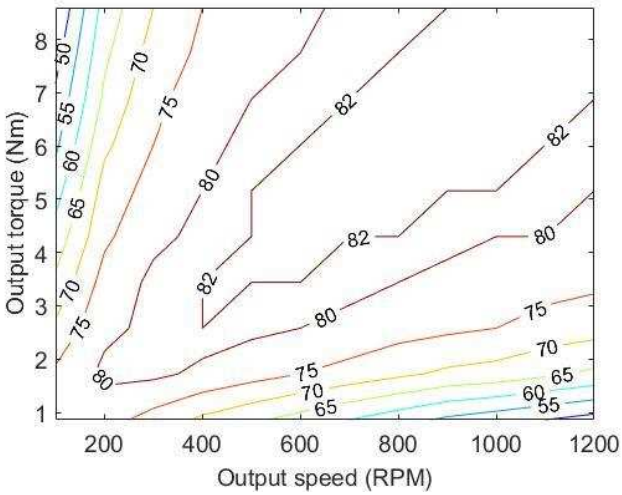

Fig. 16. Efficiency at Active Passive operation

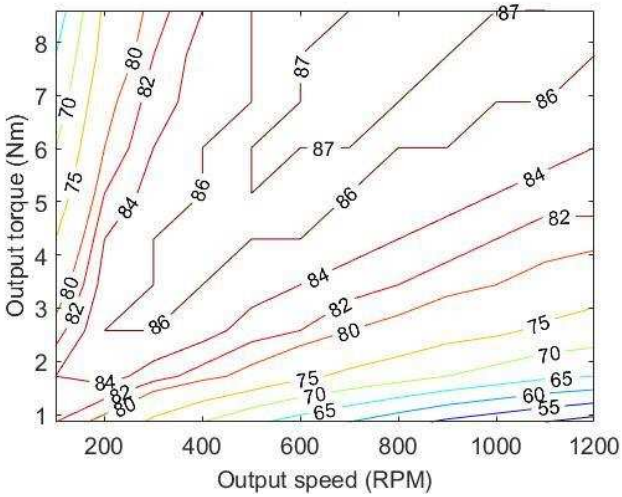

Fig. 17. Efficiency at Active-Active operation

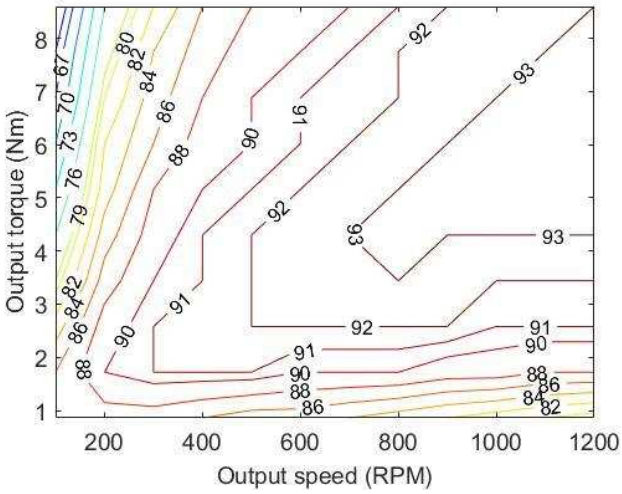

Fig. 18. Efficiency at Active-Active operation without loss of solid components

V. Comparison with conventional PM electrical machine

The stator of the fault tolerant (FT) duplex 3-phase PDD was modified in order to incorporate a non-fault tolerant (NFT) concentrated double layer 3-phase winding configuration. The NFT PDD, Fig. 19, was designed to have the same copper loss as the FT variant.

The PDDs are compared with an off the shelf aerospace approved frameless non-fault tolerant PM motor [12], which produces the same continuous torque as the PDDs. Table II, compares the 3 electrical machines, where it can be seen that in addition to the significant reduction in mass, the inertia of the PDD connected to the mechanical drivetrain, is only 6.2% of the inertia of the conventional PM machine. The low inertia of the output rotor combined with the torque limiting characteristic of the magnetic gear element has the benefit of reducing the mass and size of the end stops normally utilised in the actuator. The end stops are typically sized to absorb the kinetic energy associated with an actuator runaway condition due to loss of control.

VI. Experimental investigation

The PDD prototype test setup, Fig. 19, consists of a conventional PM machine (left) connected to the FT PDD (right) through a torque transducer. The parameters of the manufactured fault tolerant PDD electrical machine are given in Table III.

A comparison of the open circuit back-EMF of one lane of the duplex 3-phase winding configuration, at 600 rpm PPR speed, is shown in Fig. 20. Fig. 21 shows the harmonic components of the predicted and measured back-EMF waveforms. It can be observed that a good agreement exists between the 3D FE and measured with the 2D FE fundamental being 12% higher than measured. Fig. 22 shows the variation of output torque with the phase current of one 3-phase lane. The output torque is predicted using 3D magnetostatic finite element. It can be observed that due to the drag torque generated by the induced eddy currents in the solid components, i.e. Titanium sleeve, permanent magnets and solid pole-pieces, the difference between predicted and measured torque is increased with speed, albeit the slope of the torque-current characteristics remains fairly constant.

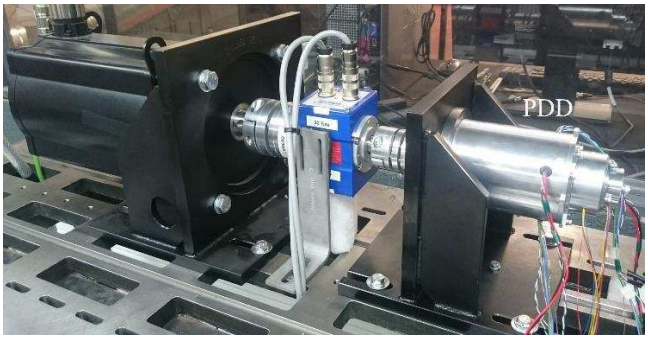

Fig. 19. PDD prototype

TABLE II. Comparison of PM and PDD electrical machines

Motor type	KBM25 [12]	FT PDD	NFT PDD
Cont. torque (Nm)	8.7	8.6	8.6
Rated cont. power (W)	1765	1080	1080
Speed at rated power (RPM)	2300	1200	1200
Inertia output rotor (kg.cm^2)	6.78	0.42	0.42
Stator outer diam. (mm)	110.0	73.8	62.8
Active length (mm)	93.7	53	53
Active mass (kg)	3.50	1.78	1.05
Torque per active vol. (Nm/l)	9.80	37.90	53.40
Torque per active mass (Nm/kg)	2.50	4.83	8.20

TABLE III. Parameters of PDD prototype

Parameter	Value
Stator outer diameter	74 mm
PPR outer diameter	45 mm
Active length	53 mm
HSR PM thickness	10 mm
Stator PM thickness	1.5 mm
PM material Sm_2Co_{17}	Recoma 28
Pole piece thickness	2 mm
Inner / Outer airgap thickness	0.7mm
Active mass	1.8 kg
Rated speed	1200 rpm
Gear ratio	7.75:1
Pull-out torque	10.3 Nm
HSR inertia	1.1×10^{-4} kgm^2
PPR inertia	4.2×10^{-5} kgm^2
HSR pole pairs	4
Stator slots	12
DC link voltage	270 VDC
Phase resistance	0.66 Ω
Phase inductance	1.87 mH
Slot current density	7.2 A_{rms}/mm^2
Number of turns	54

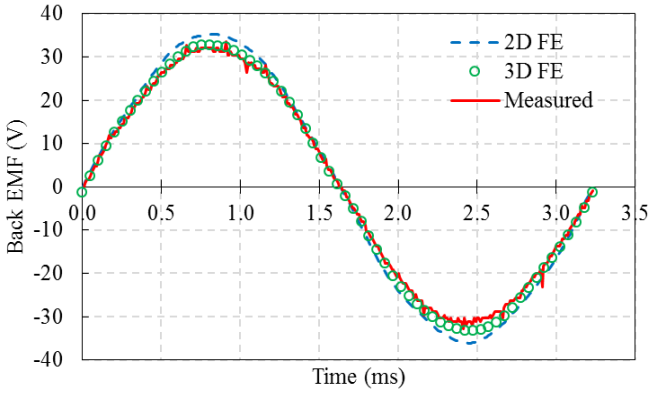

Fig. 20. PDD back-EMF 600rpm output speed

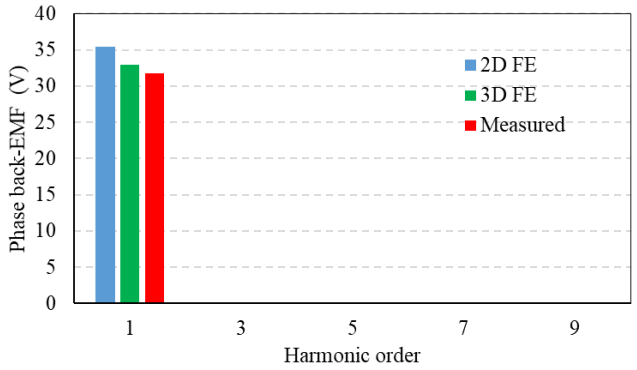

Fig. 21. Harmonic spectrum of back-EMF

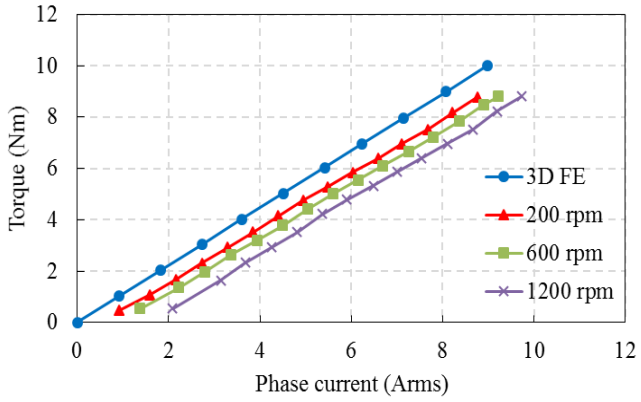

Fig. 22. Variation of output torque with input current

Fig. 23 shows the input PDD phase current and output PPR torque during steady state Active-Passive operation for a constant load torque with an average of 10.53 Nm. When the load torque is increased past the maximum torque transmission capability of the PDD, the electrical machine integrated magnetic gear slips and transmits an average torque of 0 Nm to the load. Fig. 24 shows the measured output PDD torque and phase current during a PDD pull-out condition, with the average transmitted torque of 0 Nm and reduced phase current demand.

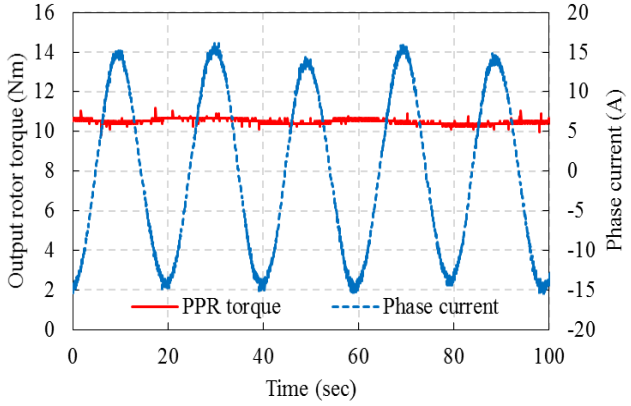

Fig. 23. PDD output torque and phase current before pull-out

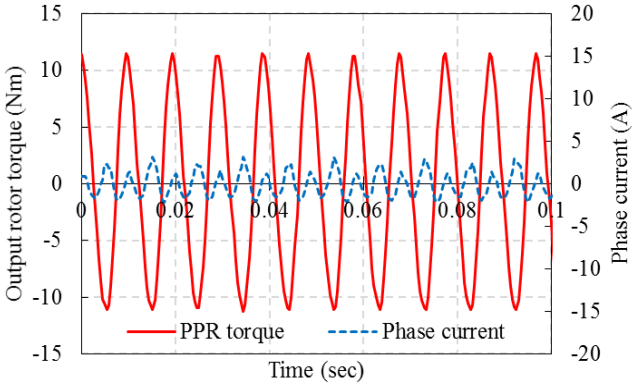

Fig. 24. PDD output torque and current during pull-out

A load servo machine having the total inertia comparable to that of the rudder surface and the mechanical drive train, referred to the output of the PDD, was used to assess the bandwidth of the prototype actuator. The position of the fault tolerant PDD was controlled using DSpace and a duplex 3-phase drive based on Texas Instruments HVMotorCtrl+PFC development kits. In order to mimic the rudder surface position dependent aerodynamic load, the sinusoidal load torque demand to the servo machine, was set through DSpace. Fig. 25 shows measured 5Hz sinusoidal angular displacement of PDD and corresponding linear slide displacement, while, Fig. 26 shows the measured load torque.

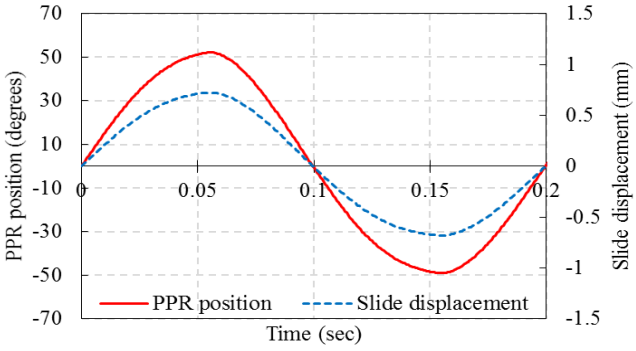

Fig. 25. Variation of PPR position and slide displacement

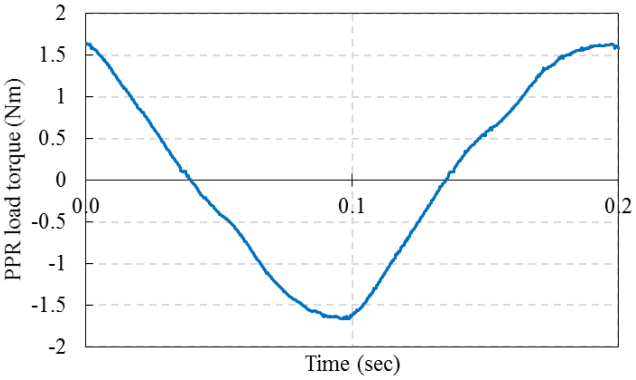

Fig. 26. Variation of PDD output torque

Fig. 27 compares the required, analytically predicted and measured bandwidth. It can be observed that the prototype fault tolerant PDD achieved a bandwidth that exceeds the requirement and a good agreement exists between the measurements and analytical predictions.

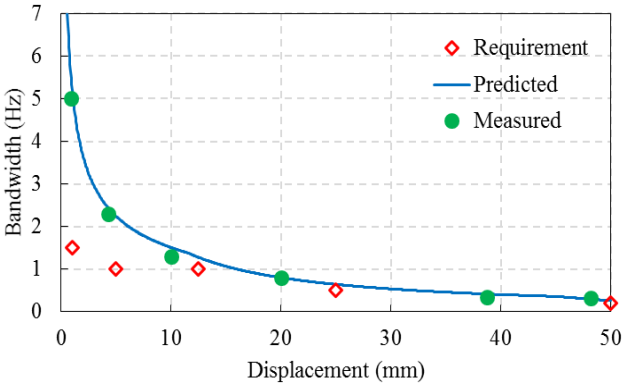

Fig. 27. Bandwidth capability of emulated actuator

VII. Conclusions

The application of a fault tolerant PDD electrical machine for flight control electromechanical actuation is investigated. It is shown that in addition to enabling a significantly lower mass solution, a PDD can exhibit an order of magnitude lower referred inertia, compared to direct-drive off the shelf electrical machines or geared motor solutions. Thus, its application should reduce the probability of jamming in the mechanical drivetrain, due to the failures caused by the kinetic energy stored in the electrical machine. The electromagnetic losses were also presented together with the efficiency maps for Active-Active and Active-Passive operation modes of the duplex 3-phase fault tolerant winding configuration. Although the efficiency is reduced by adopting solid pole pieces, which facilitates the manufacture and results in more robust solution, and a Titanium sleeve, they introduce passive damping which would improve the controllability and the stability of the actuator as well as reduce the size of the electrical damping components, such as braking resistors. Furthermore, despite the compliance of the magnetic gear of the PDD, it is shown the actuator can meet and exceed the required bandwidth.

Acknowledgements

The research was supported by Innovate UK and the Royal Commission for the Exhibition of 1851 as part of the Industrial fellowship scheme.

References

[1] B. Sarlioglu and C. T. Morris, "More Electric Aircraft: Review, Challenges, and Opportunities for Commercial Transport Aircraft," Transportation Electrification, IEEE Transactions, vol. 1, pp. 54-64, 2015.

[2] R. S. Dragan, R. E. Clark, E. K. Hussain, K. Atallah and M. Odavic, "Magnetically geared pseudo direct drive for safety critical applications," 2017 IEEE International Electric Machines and Drives Conference (IEMDC), Miami, FL, 2017, pp. 1-8.

[3] L. L. Wang, J. X. Shen, Y. Wang and K. Wang, "A novel magnetic-geared outer-rotor permanent-magnet brushless motor," 2008 4th IET Conference on Power Electronics, Machines and Drives, York, 2008, pp. 33-36.

[4] P. O. Rasmussen, H. H. Mortensen, T. N. Matzen, T. M. Jahns and H. A. Toliyat, "Motor integrated permanent magnet gear with a wide torque-speed range," 2009 IEEE Energy Conversion Congress and Exposition, San Jose, CA, 2009, pp. 1510-1518.

[5] H. Wagner, G. Nikolov, A. Bierig, and H. Spangenberg, "Challenges for Health Monitoring of Electromechanical Flight Control Actuation Systems," SAE Int. J. Aerosp., vol. 4, pp. 1316-1323, 2011.

[6] E. K. Hussain, K. Atallah, M. Odavic, R. S. Dragan and R. E. Clark, "Pseudo Direct Drive electrical machines for flight control surface actuation," 8th IET International Conference on Power Electronics, Machines and Drives (PEMD 2016), Glasgow, pp. 1-6, 2016.

[7] K. Atallah, J. Rens, S. Mezani and D. Howe, "A Novel "Pseudo" Direct-Drive Brushless Permanent Magnet Machine," in IEEE Transactions on Magnetics, vol. 44, no. 11, pp. 4349-4352, Nov. 2008.

[8] Z. Q. Zhu, D. Howe, "Influence of design parameters on cogging torque in permanent magnet machines", IEEE Trans. Magn., vol. 15, no. 5, pp. 407-412, May 2000.

[9] G. Qi, J. T. Chen, Z. Q. Zhu, D. Howe, L. B. Zhou and C. L. Gu, "Influence of skew and cross-coupling on d- and q-axis inductances and flux-weakening performance of PM brushless AC machines," 2008 International Conference on Electrical Machines and Systems, Wuhan, 2008, pp. 2854-2859

[10] W. Q. Chu and Z. Q. Zhu, "Analytical modeling and investigation of transient response of PM machines with 3-phase short-circuit fault," 2011 IEEE International Electric Machines & Drives Conference (IEMDC), Niagara Falls, ON, 2011, pp. 125-130.

[11] P. Arumugam, T. Hamiti and C. Gerada, "Fault tolerant winding design — A compromise between losses and fault tolerant capability," 2012 XXth International Conference on Electrical Machines, Marseille, 2012, pp. 2559-2565.

[12] Kollmorgen (2017,Jan. 10), Kollmorgen Frameless Motor Selection Guide [Online]. Available: http://www.kollmorgen.com/en-gb/products/motors

Radu S. Dragan received the MEng degree in Electronic and Electrical Engineering from the University of Sheffield, England, in 2014, where he is currently working towards the Ph.D degree in Electrical Engineering. His research topic is magnetic gears and Pseudo Direct Drive motors for safety critical application. Apart from his reasearch, Radu is also employed as an electrical design engineer at Magnomatics Ltd., a company dedicated to the development and manufacture of high efficiency magnet gears, magnetically-geared motors and generators and magnetic powersplit transmissions for hydrid vehicles.

Richard E. Clark obtained his first degree in Electrical Engineering from the University of Sheffield and received a Ph.D. in 1999 for research on permanent magnet actuators. Following several years as a post-doctoral Research Associate, he was awarded a 5 year Royal Academy of Engineering Research Fellowship and became a Lecturer in Electrical Engineering at the University of Sheffield in 2005. In 2007 he joined Magnomatics, a University of Sheffield spin-out company developing novel electrical motor and generators and magnetic transmissions, where he held posts of R&D Manager, Research Director and Principal Engineer.

E. K. Hussain (M'12) was born in Assiut, Egypt, He received the M.Sc. degree in Electrical Engineering from Assiut University, Assiut, Egypt, in 2003 and Ph.D. degree in Electrical Engineering from University of Sheffield, Sheffield, UK, in 2013. He worked as a Research Associate at the University of Sheffield, UK, from 2013 to 2017. Since 2018, he has been working at Exeter University, Penryn, UK, as a Business Research Fellow. His main interests include Micro-grid, Machine Drives, Renewable Energy Sources, Energy Storage Systems and More Electric Aircraft (MEA).

Milijana Odavic (M'13) received the M.Sc. degree in electrical and electronic engineering from the University of Zagreb, Zagreb, Croatia, in 2004 and the Ph.D. degree in electrical engineering from the University of Nottingham, Nottingham, U.K., in 2008. In 2013, she became a Lecturer in power electronics in the Electronic and Electrical Engineering Department, University of Sheffield, Sheffield, U.K. Prior to joining the University of Sheffield, she was a Research Fellow in the Power Electronics, Machines and Control Group, University of Nottingham and in the Department of Electric Machines, Drives and Automation, University of Zagreb. Dr Odavic's research is in the area of power electronics with particular focus on power conversion topologies, electronic power distribution systems and modelling and control.

Kais Atallah received the degree of Ingenieur d'Etat in Electrical Engineering from Ecole Nationale Polytechnique, Algeria, 1988, and the Ph.D. from the University of Sheffield, England, in 1993. He is currently a Professor of Electrical Engineering at the University of Sheffield. From 1993 to 2000 he was a Postdoctoral Research Associate in the Department of Electronic & Electrical Engineering at the University of Sheffield. In 2006, he co-founded Magnomatics Ltd., where he was Director until July 2008. His research interests embrace fault-tolerant permanent magnet drives for safety-critical applications, magnetic gearing and 'pseudo' direct drive electrical machines, and drive-trains for wind/tidal turbines and electrical/hybrid vehicles.